Published in final edited form as:
J Surg Res. 2013 July ; 183(1): 258–269. doi:10.1016/j.jss.2012.12.017.

3D quantitative ultrasound for detecting lymph-node metastases

Emi Saegusa-Beecroft, MD[1,6], **Junji Machi, MD PhD FACS**[1], **Jonathan Mamou, PhD**[2], **Masaki Hata, MD PhD**[3], **Alain Coron, PhD**[4,5], **Eugene T. Yanagihara, MD FCAP**[6], **Tadashi Yamaguchi, PhD**[7], **Michael L. Oelze, PhD**[8], **Pascal Laugier, PhD**[4,5], and **Ernest Feleppa, PhD FAIUM FAIMBE**[2]

[1]Department of Surgery, University of Hawaii and Kuakini Medical Center, Honolulu, HI

[2]Lizzi Center for Biomedical Engineering, Riverside Research, New York, NY

[3]Department of Surgery, Juntendo University School of Medicine, Tokyo, Japan

[4]University Pierre and Marie Curie University Paris 06, UMR 7623, LIP, F-75005, Paris, France

[5]Centre National de la Recherche Scientifique, UMR 7623, Laboratoire d'Imagerie Paramétrique, F-75006, Paris, France

[6]Department of Pathology, Kuakini Medical Center, Honolulu, HI

[7]Research Center for Frontier Medical Engineering, Chiba University, Chiba, Japan

[8]Department of Electrical and Computer Engineering, University of Illinois, Urbana, Ill

Abstract

BACKGROUND—Detection of metastases in lymph nodes (LNs) is critical for cancer management. Conventional histological methods may miss metastatic foci. Currently, no practical means of entire LN-volume evaluation exists. The aim of this study is to develop fast, reliable, operator-independent, high-frequency, quantitative-ultrasound (QUS) methods for evaluating LNs over their entire volumes for effectively detecting LN metastases.

MATERIALS AND METHODS—Freshly excised LNs were scanned at 26 MHz and echo-signal data were digitally acquired over the entire three-dimensional (3D) volume. 146 LNs of colorectal-, 26 LNs of gastric-, and 118 LNs of breast-cancer patients were enrolled. LNs were step-sectioned at 50-μm intervals and later compared to 13 QUS estimates associated with tissue microstructure. Linear-discriminant analysis classified LNs as metastatic or non-metastatic, and areas (Az) under receiver-operator characteristic (ROC) curves were computed to assess classification performance. QUS-estimates and cancer-probability values derived from discriminant analysis were depicted in 3D images for comparison with 3D histology.

RESULTS—23/146 LNs of colorectal-cancer patients were metastatic; Az = 0.952 ± 0.021 (95% CI: 0.911 to 0.993); sensitivity 91.3% (specificity 87.0%); sensitivity 100% (specificity 67.5%). 5/26 LNs of gastric-cancer patients were metastatic; Az = 0.962 ± 0.039 (95% CI: 0.807 to 1.000);

Corresponding author: Emi Saegusa-Beecroft, MD, Department of General Surgery, University of Hawaii and Kuakini Medical Center. Address: c/o Junji Machi, MD, PhD, 405 N. Kuakini St, Suite 601, Honolulu HI 96817, USA, Phone: 808-440-2250, Fax: 808-596-0370, esaegusa@hawaii.edu; emisaegusabeecroft@gmail.com.

Presented at the American College of Surgeons 97th Annual Clinical Congress, San Francisco, CA, October 2011.

sensitivity 100% (specificity 95.3%). 17/118 LNs of breast-cancer patients were metastatic; Az = 0.833 ± 0.047 (95% CI: 0.741 to 0.926); sensitivity 88.2% (specificity 62.5%); sensitivity 100% (specificity 50.5%). 3D cancer-probability images showed good correlation with 3D histology.

CONCLUSIONS—These results suggest that operator- and system-independent QUS methods will allow reliable entire-volume LN evaluation for detecting metastases. 3D cancer-probability images can help pathologists identify metastatic foci that could be missed using conventional methods.

Keywords

Three-dimensional quantitative ultrasound; high-frequency ultrasound; lymph-node metastases; lymph-node micrometastases; breast cancer; colorectal cancer; gastric cancer; prospective cohort study; step-sectioning histology

INTRODUCTION

For many cancers, accurate detection of metastases in lymph nodes (LNs) is crucial to determine the disease stage using the American Joint Committee on Cancer tumor-node-metastases (TNM) staging system. Changes in the N status affect treatment and management. The latest edition categorizes micrometastases (0.2 to 2 mm) and isolated tumor cells (<0.2 mm, or less than 1000 tumor cells) separately from macrometastases. Micrometastases are considered to be clinically significant and “positive” for metastases (1).

For all cancers, pathologists currently perform a microscopic histological examination of surgically dissected LNs. For colorectal cancer and gastric cancer, only one central histological section of each LN is usually evaluated for metastases, regardless of LN size (2, 3). For invasive carcinoma of the breast, the College of American Pathologists recommends that each LN should be sliced parallel to the long axis of the LN at a spacing of 2 mm. These slices are then submitted for microscopic examination with at least one representative hematoxylin and eosin (H&E)-stained thin section obtained from the surface of each slice examined histologically (4).

Currently, no method is clinically available for examining LNs in their entire volume to detect metastases. Molecular studies such as reverse transcription polymerase chain reaction have been reported (5-8), but continue to be a research topic and have not been adopted for clinical practice. There is some consensus in the literature that treatment decisions should not yet be based on these techniques (1,2,3,4,9-12). The gold standard remains histologic examination of H&E histology, and occasionally additional sections from the specimen may be required for subsequent special staining such as immunohistochemical methods (4,13,14). With the conventional method, unless the metastases are included in the section examined microscopically, metastases, particularly micrometastases, may be missed (15-22).

Breast sentinel LN biopsy now is well established in the US for clinically node-negative axillas (23,24). Touch-prep imprinting and frozen-section procedures for detection of metastases provide limited sensitivity because of sampling limitations (24-29). Multiple-level step sectioning of specimens has been reported to detect more metastases (15-18,20-22). Different countries and facilities have reported their own protocols for multiple-level step sectioning at different intervals of axillary sentinel LNs of breast-cancer patients (4,30-32), but currently no international consensus on an optimal histopathology procedure exists (32). The clinical impact on the outcome of detecting “occult” micrometastases and isolated tumor cells remains controversial (4,17,21,33-36). Recently, the necessity for completing a formal axillary LN dissection in patients with a positive sentinel LN biopsy showing macro- or micrometastases in less than three nodes has been

questioned (37) and remains controversial (38). However, many of these studies do not account for the potential true residual disease prevalence in axillary LNs because metastases are detected using limited conventional histopathological procedures. If a new method could be developed to rapidly assess LNs for suspicion of metastases in a non-invasive way, over the entire LN volume prior to histology processing, then the new method would resolve the current controversies and would have broad implications for staging a wide range of cancers.

The aim of our study is to develop a fast, reliable, and operator-independent method for entire-volume LN examination to detect and image LN metastases using high-frequency (HF), quantitative-ultrasound (QUS) (39,40). By utilizing HF ultrasound (i.e., >15 MHz), and digitally acquiring and analyzing the ultrasound echo signals, QUS methods can provide estimates of tissue microstructure on a subresolution scale. Unlike B-mode ultrasound images currently used clinically, QUS methods are operator independent and provide a quantitative means of estimating microscopic-scale tissue properties. These attributes, combined with the ability of three-dimensional (3D) ultrasound scan to acquire data from the full LN volume, enable QUS methods to evaluate the entire LN and detect micro as well as macrometastases. Future clinical 3D QUS systems potentially will enable surgeons and pathologists to detect metastatic LNs with high sensitivity.

MATERIALS AND METHODS

Enrollment

A total of 160 patients (44 men and 116 women) with histologically-proven colorectal, gastric, and breast cancer who underwent cancer surgery at the Kuakini Medical Center in Honolulu, HI, USA were randomly and consecutively enrolled in this prospective study. This patient cohort included 71 patients (all women) with breast cancer, 77 patients (38 men and 39 women) with colorectal cancer, and 12 patients with gastric cancer (6 men and 6 women). The median age for each cancer type was: breast 65 years (range = 42 to 93, mean = 67.4, SD = 12.5); colorectal 74 years (range = 40 to 95, mean = 71, SD = 13.1); and gastric 81.5 years (range = 52 to 93, mean = 76.3, SD=14.1).

Institutional review boards at the University of Hawaii and the Kuakini Medical Center approved the study protocol. Written informed consent was obtained from all patients.

Materials

The study materials were LNs harvested from surgical specimens dissected from previously untreated patients with histologically proven colorectal, gastric, or breast cancer; axillary sentinel LNs that underwent an imprint (i.e., “touch-prep”) cytology procedure satisfied this criterion. The study excluded LNs with undetermined primary-cancer origins, LNs undergoing a frozen-section procedure because of potential tissue damage, large LNs that did not fit in the standard embedding cassette (3.0 cm × 2.6 cm), and LNs that were retrieved after formalin fixation or immersion in fat-clearing solutions.

LNs were harvested from freshly excised gross surgical specimens submitted to pathology for standard-of-care histological evaluation. Excess perinodal adipose tissue was carefully removed during the lymph node harvest, leaving 0.3 mm to 0.5 mm of surrounding fat layer, in order to avoid inadvertently removing lymphoid tissue. The study procedures did not interfere with the standard-of-care pathology protocol, but added additional histological information by microscopically examining each LN over its entire volume by step-sectioning instead of by conventional methods, which only examine thin sections obtained from the central plane of the node or from 2-mm-thick sections.

The investigator was independent of the surgical and the pathology service, and did not have access to clinical information. The investigator performing the dissections was informed only that the LNs were dissected from histologically-proven colorectal-, and gastric-, and breast-cancer patients, and was blinded from clinical information such as clinical presentation, history, physical examination, palpable LN status, primary tumor properties such as histological type, size, grade, etc, and was blinded. Freshly excised LNs were randomly selected from the gross surgical specimen, and were immediately submerged in 0.9% normal saline pinned to a sound-absorbing material, then scanned with HF ultrasound to acquire radiofrequency (RF) echo-signal data.

High-frequency ultrasonic data acquisition

A custom, HF ultrasound, laboratory scanning system was designed and built in order to acquire RF echo-signal data in 3D from freshly excised LNs. This system allowed LNs to be scanned over their entire volume. The scanning apparatus featured a single-element, spherically focused, ultrasound transducer (PI-30, Olympus NDT, Waltham, MA) with a 12.2-mm focal length and 6.1-mm aperture. The transducer had a center frequency of 25.6 MHz and a minus-6dB bandwidth that extended from 16.4 to 33.6 MHz. The received RF echo signals were digitized at a 400 MHz sampling frequency with an accuracy of 8 bits. Scan vectors were uniformly spaced by 25 μm in X and Y directions across the entire scan volume to acquire complete full-volume 3D data from each LN. (39,40) Typical scanning time ranged from 5 to 30 minutes, depending on the size of the LN.

Histology processing

Immediately after ultrasound data acquisition, individual dissected LNs were inked to retain orientation for subsequent reconstruction of node histology in 3D and 3D correlations with QUS results. Inked nodes were bisected and then fixed in 10% formalin for at least 6 hours, followed by paraffin processing. Nodes then were embedded into paraffin-block cassettes. In our study, a step sectioning procedure was used and 3 μm thin sections were cut at 50 μm steps from each paraffin block then stained with H&E. Two pathologists examined all slides microscopically.

Finally, fine-resolution (0.23 μm/pixel) digital photomicrographs of the slides were obtained using a virtual-digital-microscopy scanner (Hamamatsu NanoZoomer 2.0-HT, Hamamatsu City, Japan). Metastatic regions were demarcated using Hamamatsu digital editing software. 3D histology reconstruction was performed, and 3D histology was compared to 3D QUS images to train and evaluate the classifier, and to verify results.

QUS parameter estimation

In this blinded study, the acquired ultrasound data were analyzed by an investigator at Riverside Research in NY who was blinded to the histology results obtained at the Kuakini Medical Center in HI. After all analyses were completed, the QUS results and the histology results were compared. As described in previous publications, QUS parameters based on spectrum analysis and envelope statistics were estimated from the acquired RF echo-signal data (39,40). These QUS methods are only briefly summarized here.

After image segmentation to separate saline and perinodal fibroadipose tissue from the nodal region, acquired RF echo-signal data were analyzed using a series of overlapping 3D cylindrical regions of interest (ROIs) that were 1 mm long and 1 mm in diameter. An average power spectrum normalized to a water-oil interface was computed from the echo signals in the ROI to obtain four spectrum-analysis-based QUS estimates. A straight-line scattering model provided the spectral slope and spectral intercept (39). A spherical

Gaussian scattering model provided the effective scatterer size and acoustic concentration (39).

The envelopes of the RF signals within each ROI were computed, and analyses of probability-density functions of the envelope signals provided the four additional QUS estimates. Analyses included application of Nakagami and Homodyned-K statistics models to the envelope signals to derive Nakagami α and Nakagami ω from the Nakagami distribution, and Homodyned-K μ and Homodyned-K k from the Homodyned-K distribution (40). Finally, the remaining five QUS estimates were obtained using modified quantile-quantile plot. These estimates were the coordinates of the intersection of low-amplitude and high-amplitude regressions (*Cx* and *Cy*), and three slopes estimates (*Sl, Sh, Sa*) and were obtained by fitting two regression curves to the modified quantile-quantile plot. These five quantile-quantile estimates quantified the difference between the probability-density functions of the ROI and Rayleigh-distribution probability-density functions (41).

Classification

All QUS estimates and histologic examination results were used to classify cancerous and non-cancerous LNs using linear-discriminant analysis. Linear-discriminant analysis combined the 13 different QUS estimates to maximize the differentiation between benign and metastatic tissue in cancer-free and cancer-filled LNs using 50-μm step-sectioning histology as the gold standard. In addition, a step-wise approach was implemented to remove QUS estimates from linear-discriminant analysis when they did not significantly contribute to classification performance.

Histologic differences between LNs of colorectal- and gastric-cancer patients compared to LNs of breast-cancer patients affect the associated QUS estimates for each type of LN metastasis. Consequently, distinct classifiers were obtained for LNs of colorectal- and gastric- vs. breast-cancer rather than across the entire sample population. Classifier quality was expressed as the area under a receiver-operator characteristics curve (Az). The Az values provided quantitative comparisons of classifier performance for different combinations of QUS estimates.

An interactive graphical user interface (GUI) was developed to permit virtual 3D dissection and exploration of freshly dissected LNs; the GUI displays linked, orthogonal, mouse-selected cross-sectional views of the node with a histology plane that matches the XY ultrasound plane. The interactive display consisted of a gray scale B-mode plane of the 3D volume with overlaid color-encoded QUS-estimate or cancer-probability values. Cancer probabilities were estimated using a Bayesian approach based on the discriminant score, which is described in detail in our previous study (42).

RESULTS

Classification performance

Table 1 shows Az values for classification of 290 LNs from 160 patients based on linear-discriminant analysis of the QUS-estimate values. The table also indicates the type of primary cancer and the QUS estimates used as classifiers for each Az value.

Figure 1 displays the ROC curves for LNs of the three cancer types. The ROC curves make the superior classification performance for colorectal and gastric cancers compared to breast cancer readily apparent.

23 of 146 LNs of colorectal-cancer patients were metastatic. As shown in Fig. 1, linear-discriminant analysis gave an Az of 0.952 ± 0.021 (95% CI: 0.911 to 0.993); sensitivity

91.3% (corresponding specificity 87.0%). 5 of 26 LNs of gastric-cancer patients were metastatic; linear-discriminant analysis gave an Az of 0.962 ± 0.039 (95% CI: 0.807 to 1.000). 17 of 118 LNs of breast-cancer patients were metastatic; linear-discriminant analysis gave an Az of 0.833 ± 0.047 (95% CI: 0.741 to 0.926); sensitivity 88.2% (corresponding specificity 62.5%). As indicated by the Az values, excellent classification was achieved for LNs of colorectal-cancer and gastric-cancer patients. The total number of LNs analyzed for gastric cancer is less than the number of LNs analyzed for colorectal cancer and breast cancer. The classification performance of LNs of colorectal-cancer patients was superior to the classification achieved for axillary LNs of breast cancer patients; however, the breast-cancer classification results were still satisfactory.

Illustrative QUS images

Examples of QUS information expressed as 3D images of QUS-estimate values are shown in Figs. 2 and 3. These figures respectively illustrate QUS-estimate images of representative benign LNs and diffusely metastatic LNs of colorectal- and gastric-cancer patients. Segmentation results are color-encoded in green and red. The figures show parametric cross-sectional images displaying effective scatterer-size estimates in three orthogonal planes within the 3D volume. The H&E-stained histology shown in the lower right corresponds to the scatterer-size image plane shown in the lower left.

Average effective scatterer-size estimates were 22.96 μm for the benign LN shown in Figure 2-a, and 33.36 μm for the metastatic LN shown in Figure 2-b. Comparison of the two bottom panels of Figures 2-a and 2-b shows that these illustrative QUS images suggest that larger effective scatterer-size may reliably indicate metastases in LNs of colon cancer patients.

Average effective scatterer-size estimates were 28.69 μm for the benign LN shown in Figure 3-a, and 36.69 μm for the metastatic LN shown in Figure 3-b. Comparison of the 2 bottom panels of Figures 3-a and 3-b shows that these illustrative QUS images suggest that larger scatterer-size may reliably indicate metastases in LNs of gastric cancer patients.

For LNs of colorectal and gastric cancers, metastatic LNs displayed larger scatterer-size values than cancer-free LNs. These illustrative results suggest that larger scatterer-size may reliably indicate metastases in LNs of patients with colorectal cancer and gastric cancer. This shows how even a single QUS estimate alone, scatterer-size, could aid in identifying suspicious regions.

3D Interactive GUI with cancer-probability images and depiction of micrometastases

A custom GUI displayed 3D QUS and matching 3D histology images for virtual LN interactive evaluation. Figures 4-1 and 5-1 show screen captures from this GUI for a partially metastatic LN from a colorectal-cancer patient and a LN from a breast-cancer patient with micrometastases, respectively. Figures 4-2 and 5-2 show screen captures from this GUI for a benign LN from a colorectal-cancer patient and a benign LN from a breast-cancer patient, respectively. The GUI displays three conventional B-mode ultrasound images from orthogonal planes X, Y, and Z augmented with overlaid color-coded cancer probability. The lower-right image displays the co-registered XY-plane histology with green outlining cancerous regions indicated in Figures 4-1 and 5-1. Comparisons of the XY-plane QUS cancer-probability B-mode image with the histology image shows an excellent match between the QUS-based depiction of cancerous regions and the histologically determined micro- and macro-metastatic foci. In contrast to Figures 4-1 and 5-1, Figures 4-2 and 5-2 illustrate how the region classified by QUS-based depiction of cancer-probability of less than 25% matches the histologically proven benign regions.

DISCUSSION

Evolution of metastases detection in LNs using high-frequency QUS methods

Conventional, clinical, B-mode ultrasound images (<15 MHz) are qualitative, operator and system dependent. Because QUS processing exploits information present in the RF echo signals that is discarded by conventional ultrasound image processing, QUS methods are sensitive to the microstructural features of tissue that cannot be assessed using conventional imaging methods. The theoretical framework for QUS originally was developed in the 1980s (43). Since then, QUS approaches for tissue characterization have been extended and refined (39,40,44-59). In this study, we used HF-QUS (>15 MHz) to assure sensitivity to small features of tissue microarchitecture on the scale of tens of μm. Despite limitations in penetration depth imposed on HF-QUS by frequency-dependent attenuation, the small sizes of the great majority of clinically encountered LNs makes HF-QUS applicable for guiding pathologists to suspicious regions in dissected LNs. Furthermore, in this study, excess perinodal adipose tissue was carefully removed during the lymph node retrieval procedure, leaving 0.3 mm to 0.5 mm of surrounding fat layer. In addition to minimizing the attenuation issue, this approach ensured that the entire nodal volume was adequately sampled for entire-volume histology processing. Although the excess perinodal fat layer was removed for this study, we believe that we can better address attenuation concerns once a dedicated system is developed, e.g., by optimizing transmitted power and frequency to increase the penetration depth. In an optimized system, the proposed QUS methods may be potentially applicable to freshly excised surgical specimens, such as colectomy specimens and breast axillary lymph node dissection specimens, prior to the lymph-node harvest performed by pathologists.

During the early stages of our present study, our group described the basis for 3D HF-QUS methods of LN tissue characterization (39). Previous studies using linear-discriminant analysis demonstrated that just two of the 13 QUS estimates, effective scatterer size and the k parameter using the Homodyned-K distribution, were sufficient to reliably distinguish cancerous from cancer-free LNs of patients with colorectal cancer and gastric cancer. By utilizing these two QUS classifiers alone, 95.0% sensitivity was achieved with 95.7% specificity (40).

Our latest results suggest that HF-QUS methods can reliably identify regions of LNs that are suspicious for LN metastases of all three cancer-types investigated. Identification of suspicious LNs was successful not only for diffusely metastatic LNs, but also for LNs with micrometastases.

In our previous studies, all colorectal- and gastric-cancer patients enrolled had adenocarcinomas. LNs of both colorectal- and gastric-cancer patients were analyzed together because of the histologic similarity between these types of LNs and few numbers of enrolled gastric-cancer patients (40). Metastatic colorectal cancer and gastric cancer in LNs had larger QUS effective scatterer-size compared to benign LNs. In general, tumor cells are larger than lymphocytes. This may explain the larger QUS estimate of effective scatterer size observed in metastatic LNs of colorectal- and gastric-cancer patients compared to benign LNs. The LN metastases of other cancers are known to have different microscale morphology; for example, LNs of breast-cancer patients often present with fatty ingrowths. The variability of axillary LN morphology is well known, and attenuation through the fatty ingrowth in axillary LNs of breast-cancer patients, compared to LNs of colorectal-cancer patients, may degrade QUS-based classification. This suggests that different QUS estimate combinations may be more effective for detecting regions suspicious for metastases for different types of primary tumors.

Interactive 3D Cancer-probability images as a future pathology tool

Interactive 3D cancer-probability images based on HF ultrasound can be made into a small low-cost pathology tool that can scan LNs immediately after the surgical specimen is received in the pathology laboratory. In this study, a custom research scanning system was used. The scanning time varied between 5 and 30 minutes depending on the size of the lymph node. However, once this method is incorporated into a dedicated system with much faster motors, we believe that the scanning time can be shortened to less than 2 minutes per lymph node for an entire volume 3D nodal examination.

This will provide a fast, reliable, and operator-independent technique that can scan fresh LNs and provide interactive real-time B-mode ultrasound images with color-encoded cancer-probability overlays as shown in Figs. 4 and 5. The LNs also can be scanned intra-operatively immediately following lymphadenectomy or excision of the surgical specimen while the specimen remains intact. This may benefit cancer management by aiding decisions that depend on LN status, e.g., on the number of total metastatic LNs. This tool may assist in detecting small metastatic foci that would be missed by standard, intra-operative, touch-prep or frozen section procedures, which is especially important for breast cancer sentinel LN biopsy. If QUS-based, cancer-probability images show regions that are highly suspicious for metastases, e.g., regions with a cancer probability of more than 75%, then the pathologist can target the intra-operative touch-prep procedure or frozen section procedure to those highly suspicious regions. Also, the operator would be able to adjust the sensitivity and specificity to establish a preferred threshold for decision choices, e.g., to obtain 100% sensitivity with the corresponding specificity. The first potential use for this novel tool would be to guide pathologists to suspicious regions of LNs for definitive histology; if successful, it potentially can dramatically improve detection sensitivity to small metastatic foci that would be missed using conventional histology methods.

This study was limited by the relatively low enrollment of gastric cancer patients, compared to colorectal cancer patients. Future enrollment of additional gastric cancer patients may confirm results obtained to date with LNs of colorectal cancer patients. The total number of LNs acquired per enrolled cancer patient also limited the study. Only freshly excised LNs were selected, which excluded LNs harvested after formalin fixation or exposure to fat-dissolving solutions. To avoid delay in diagnosis, which may interfere with the standard of care, we limited the number of LNs processed using our full-volume step-sectioning. As a prospective study, selection bias was precluded by sequentially enrolling patients, by randomly selecting LNs for the study from the full surgical specimen, and by blinding the investigator who selected the LNs from the specimen to clinical information.

In addition to continuing data acquisition and improving the QUS methods, additional studies are being planned to apply these QUS methods to lower ultrasound frequencies to assess their applicability to LN evaluations *in-situ*. Our group plans to develop a low cost interactive small pen-type device based on these results that can instantaneously scan LNs and provide cancer-probability results within seconds. The *in-situ* application is intended to enable surgeons to identify suspicious axillary sentinel LNs of breast-cancer patients in the operating room. This potential device will use a lower frequency to avoid frequency-dependent attenuation challenges at higher frequencies, and will also be intended to scan non-sentinel axillary LNs of breast cancer patients. This may contribute to resolving the current controversy over sentinel LN biopsy, and consequently, may contribute to improving surgical treatment and management of breast cancer.

The *ex-vivo* application with higher ultrasound frequencies will enable pathologists to identify suspicious LNs of all three cancer-types in the pathology lab. The number of regional LN metastases changes the node status of the tumor-node-metastases staging, and

therefore affect the cancer staging and prognosis in all three cancer-types. This future pathology tool may contribute to more-sensitive detection of metastases and therefore more-accurate tumor-node-metastases staging by targeting the permanent histology section to the suspicious region.

In conclusion, our results suggest that the described 3D QUS methods can reliably detect metastases in LNs. Furthermore; these techniques may enable detection of the clinically relevant fraction of micrometastases that are missed by conventional single-section histology. The high probability of missed clinically significant metastases is of great concern because detection of all micrometastases is essential for accurate staging and effective treatment.

Acknowledgments

The authors would like to thank Gregory K. Kobayashi MD FCAP, Clifford C. Wong MD FCAP, Patricia Kim MD FCAP, and Conway Fung MT at the Departmemt of Pathology, Kuakini Medical Center, Honolulu, HI for their pathology and histology expertise. Emi Saegusa-Beecroft would like to thank Professor Keisho Marumo MD PhD, Department of Orthopedic Surgery, Jikei University School of Medicine, Tokyo, Japan for his mentorship. Research reported in this publication was supported by the National Institutes of Health under grant CA 100183 awarded to Ernest J. Feleppa, PhD. The content is solely the responsibility of the authors and does not necessarily represent the official views of the National Institutes of Health.

References

1. Edge, SB.; Byrd, DR.; Compton, CC., et al. AJCC (American Joint Committee on Cancer) Cancer Staging Manual. 7. NY: Springer- Verlag; 2010. p. 1-12.p. 117-126.p. 143-164.p. 347-376.
2. College of American Pathologists. [September 20, 2012] Protocol for the Examination of Specimens From Patients With Primary Carcinoma of the Colon and Rectum. Available at: http://www.cap.org/apps/docs/committees/cancer/cancer_protocols/2012/Colon_12protocol_3200.pdf
3. College of American Pathologists. [September 20, 2012] Protocol for the Examination of Specimens From Patients With Carcinoma of the Stomach. Available at: http://www.cap.org/apps/docs/committees/cancer/cancer_protocols/2012/Stomach_12protocol_3200.pdf
4. College of American Pathologists. [September 20, 2012] Protocol for the Examination of Specimens From Patients With Invasive Carcinoma of the Breast. Available at: http://www.cap.org/apps/docs/committees/cancer/cancer_protocols/2012/BreastInvasive_12protocol_3100.pdf
5. Viale G, Dell'Orto P, Biasi MO, et al. Comparative evaluation of an extensive histopathologic examination and a real-time reverse-transcription-polymerase chain reaction assay for mammaglobin and cytokeratin 19 on axillary sentinel lymph nodes of breast carcinoma patients. Ann Surg. 2008; 247:136–142. [PubMed: 18156933]
6. Julian TB, Blumencranz P, Deck K, et al. Novel intraoperative molecular test for sentinel lymph node metastases in patients with early-stage breast cancer. J Clin Oncol. 2008; 26:3338–3345. [PubMed: 18612150]
7. Wallwiener CW, Wallwiener M, Kurth RR, et al. Molecular detection of breast cancer metastasis in sentinel lymph nodes by reverse transcriptase polymerase chain reaction (RT-PCR): identifying, evaluating and establishing multi-marker panels. Breast Cancer Res Treat. 2011; 130:833–844. [PubMed: 21858660]
8. Nissan A, Jager D, Roystacher M, et al. Multimarker RT-PCR assay for the detection of minimal residual disease in sentinel lymph nodes of breast cancer patients. Br J Cancer. 2006; 13(94):681–685. [PubMed: 16495929]
9. Lyman GH, Giuliano AE, Somerfield MR, et al. American Society of Clinical Oncology guideline recommendations for sentinel lymph node biopsy in early-stage breast cancer. J Clin Oncol. 2005; 23:7703–7720. [PubMed: 16157938]
10. National Comprehensive Cancer Network (NCCN) guidelines. [September 20, 2012] Locoregional treatment of primary breast cancer: consensus recommendations from an International Expert Panel. Available at: www.nccn.org

11. Kaufmann M, Morrow M, von Minckwitz G, et al. Locoregional treatment of primary breast cancer: consensus recommendations from an International Expert Panel. Cancer. 2010; 116(5): 1184–1191. [PubMed: 20087962]
12. Cserni G, Bianchi S, Vezzosi V, et al. The value of cytokeratin immunohistochemistry in the evaluation of axillary sentinel lymph nodes in patients with lobular breast carcinoma. J Clin Pathol. 2006; 59:518–522. [PubMed: 16497870]
13. Weinberg ES, Dickson D, White L, et al. Cytokeratin staining for intraoperative evaluation of sentinel lymph nodes in patients with invasive lobular carcinoma. Am J Surg. 2004; 188:419–422. [PubMed: 15474439]
14. Giuliano AE, Hawes D, Ballman KV, et al. Association of occult metastases in sentinel lymph nodes and bone marrow with survival among women with early-stage invasive breast cancer. JAMA. 2011; 306(4):385–393. [PubMed: 21791687]
15. de Boer M, van Dijck JA, Bult P, et al. Breast cancer prognosis and occult lymph node metastases, isolated tumor cells, and micrometastases. J Natl Cancer Inst. 2010; 102:410–425. [PubMed: 20190185]
16. Weaver DL, Le UP, Dupuis SL, et al. Metastasis detection in sentinel lymph nodes: comparison of a limited widely spaced (NSABP protocol B-32) and a comprehensive narrowly spaced paraffin block sectioning strategy. Am J Surg Pathol. 2009; 33:1583–1589. [PubMed: 19730364]
17. Weaver DL, Ashikaga T, Krag DN, et al. Effect of occult metastases on survival in node-negative breast cancer. N Engl J Med. 2011; 364:412–421. [PubMed: 21247310]
18. Takeshita T, Tsuda H, Moriya T, et al. Clinical implications of occult metastases and isolated tumor cells in sentinel and non-sentinel lymph nodes in early breast cancer patients: serial step section analysis with long-term follow-up. Ann Surg Oncol. 2012; 19:1160–1166. [PubMed: 21989659]
19. Hata M, Machi J, Mamou J, et al. Entire-volume Serial Histological Examination for Detection of Micrometastases in Lymph Nodes of Colorectal Cancers. Pathol Oncol Res. 2011; 17:835–841. [PubMed: 21494849]
20. Boler DE, Uras C, Ince U, Cabioglu N. Factors predicting the non-sentinel lymph node involvement in breast cancer patients with sentinel lymph node metastases. Breast. 2012; 21:518–523. [PubMed: 22410110]
21. Wu Y, Mittendorf EA, Kelten C, et al. Occult axillary lymph node metastases do not have prognostic significance in early stage breast cancer. Cancer. 2012; 15(118):1507–1514. [PubMed: 22009292]
22. Grabau D, Ryden L, Fernö M, Ingvar C. Analysis of sentinel node biopsy - a single-institution experience supporting the use of serial sectioning and immunohistochemistry for detection of micrometastases by comparing four different histopathological laboratory protocols. Histopathology. 2011; 59:129–138. [PubMed: 21668472]
23. Giuliano AE, Dale PS, Turner RR, et al. Improved axillary staging of breast cancer with sentinel lymphadenectomy. Ann Surg. 1995; 222:394–401. [PubMed: 7677468]
24. Lyman GH, Giuliano AE, Somerfield MR, et al. American Society of Clinical Oncology guideline recommendations for sentinel lymph node biopsy in early-stage breast cancer. J Clin Oncol. 2005; 23:7703–7720. [PubMed: 16157938]
25. Krishnamurthy S, Meric-Bernstam F, Lucci A, et al. A prospective study comparing touch imprint cytology, frozen section analysis, and rapid cytokeratin immunostain for intraoperative evaluation of axillary sentinel lymph nodes in breast cancer. Cancer. 2009; 115:1555–1562. [PubMed: 19195040]
26. Menes TS, Tartter PI, Mizrachi H, et al. Touch preparation or frozen section for intraoperative detection of sentinel lymph node metastases from breast cancer. Ann Surg Oncol. 2003; 10:1166–1170. [PubMed: 14654472]
27. Vanderveen KA, Ramsamooj R, Bold RJ. A prospective, blinded trial of touch prep analysis versus frozen section for intraoperative evaluation of sentinel lymph nodes in breast cancer. Ann Surg Oncol. 2008; 15:2006–2011. [PubMed: 18481152]
28. Guidroz JA, Johnson MT, Scott-Conner CE, et al. The use of touch preparation for the evaluation of sentinel lymph nodes in breast cancer. Am J Surg. 2010; 199:792–796. [PubMed: 19954770]

29. van de Vrande S, Meijer J, Rijnders A, Klinkenbijl JH. The value of intraoperative frozen section examination of sentinel lymph nodes in breast cancer. Eur J Surg Oncol. 2009; 35:276–280. [PubMed: 18786801]
30. Veronesi U, Paganelli G, Viale G, et al. Sentinel-lymph-node biopsy as a staging procedure in breast cancer: update of a randomised controlled study. Lancet Oncol. 2006; 7:983–990. [PubMed: 17138219]
31. Cserni G, Amendoeira I, Apostolikas N, et al. Discrepancies in current practice of pathological evaluation of sentinel lymph nodes in breast cancer. Results of a questionnaire based survey by the European Working Group for Breast Screening Pathology. J Clin Pathol. 2004; 57:695–701. [PubMed: 15220360]
32. Van Diest PJ, Torrenga H, Borgstein PJ, et al. Reliability of intraoperative frozen section and imprint cytological investigation of sentinel lymph nodes in breast cancer. Histopathology. 1999; 35:14–18. [PubMed: 10383709]
33. Gobardhan PD, Elias SG, Madsen EV, et al. Prognostic value of lymph node micrometastases in breast cancer: a multicenter cohort study. Ann Surg Oncol. 2011; 18:1657–1664. [PubMed: 21153885]
34. Chen SL, Hoehne FM, Giuliano AE. The prognostic significance of micrometastases in breast cancer: a SEER population-based analysis. Ann Surg Oncol. 2007; 14:3378–3384. [PubMed: 17899293]
35. Reed J, Rosman M, Verbanac KM, et al. Prognostic implications of isolated tumor cells and micrometastases in sentinel nodes of patients with invasive breast cancer: 10-year analysis of patients enrolled in the prospective East Carolina University/Anne Arundel Medical Center Sentinel Node Multicenter Study. J Am Coll Surg. 2009; 208:333–340. [PubMed: 19317993]
36. Pepels MJ, de Boer M, Bult P. Regional recurrence in breast cancer patients with sentinel node micrometastases and isolated tumor cells. Ann Surg. 2012; 255(1):116–121. [PubMed: 22183034]
37. Giuliano AE, Hunt KK, Ballman KV, et al. Axillary dissection vs no axillary dissection in women with invasive breast cancer and sentinel node metastasis: a randomized clinical trial. JAMA. 2011; 305:569–575. [PubMed: 21304082]
38. Carlson GW, Wood WC. Management of axillary lymph node metastasis in breast cancer: making progress. JAMA. 2011; 305:606–607. [PubMed: 21304087]
39. Mamou J, Coron A, Hata M, et al. Three-dimensional high-frequency characterization of cancerous lymph nodes. Ultrasound Med Biol. 2010; 36:361–375. [PubMed: 20133046]
40. Mamou J, Coron A, Oelze M, et al. Three-dimensional high-frequency backscatter and envelope quantification of cancerous human lymph nodes. Ultrasound Med Biol. 2011; 37:345–57. [PubMed: 21316559]
41. Yamaguchi T, Hachiya H. Proposal of a parametric imaging method for quantitative diagnosis of liver fibrosis. Journal of Medical Ultrasonics. 2012; 37(4):155–166.
42. Mamou J, Saegusa-Beecroft E, Coron A, et al. Three-dimensional quantitative ultrasound to guide pathologists towards metastatic foci in lymph nodes. Proceedings of the annual International Conference of the IEEE EMBS. 2012:1114–1117. [PubMed: 23366091]
43. Lizzi FL, Greenebaum M, Feleppa EJ, et al. Theoretical framework for spectrum analysis in ultrasonic tissue characterization. J Acoust Soc Am. 1983; 73:1366–1373. [PubMed: 6853848]
44. Feleppa EJ, Lizzi FL, Coleman DJ, Yaremko MM. Diagnostics spectrum analysis in ophthalmology: a physical perspective. Ultrasound Med Biol. 1986; 12:623–63. [PubMed: 3532476]
45. Insana MF, Wagner RF, Brown DG, Hall TJ. Describing small-scale structure in random media using pulse-echo ultrasound. J Acoust Soc Am. 1990; 87:179–192. [PubMed: 2299033]
46. Insana MF, Hall TJ. Parametric ultrasound imaging from backscatter coefficient measurements: image formation and interpretation. Ultrason Imaging. 1990; 12:245–67. [PubMed: 1701584]
47. Feleppa EJ, Machi J, Noritomi T, et al. Differentiation of metastatic from benign lymph nodes by spectrum analysis in vitro. Proceedings of the 1997 IEEE Ultrasonics Symposium. 1997:1137–1140.

48. Oelze ML, Zachary JF, O'Brien WD Jr. Characterization of tissue microstructure using ultrasonic backscatter: Theory and technique for optimization using a Gaussian form factor. J Acoust Soc Am. 2002; 112:1202–1211. [PubMed: 12243165]

49. Kolios MC, Czarnota GJ, Lee M, et al. Ultrasonic spectral parameter characterization of apoptosis. Ultrasound Med Biol. 2002; 28:589–597. [PubMed: 12079696]

50. Mamou J, Oelze ML, O'Brien WD Jr, Zachary JF. Identifying ultrasonic scattering sites from three-dimensional impedance maps. J Acoust Soc Am. 2005; 117:413–423. [PubMed: 15704434]

51. Baddour RE, Sherar MD, Hunt JW, et al. High-frequency ultrasound scattering from microspheres and single cells. J Acoust Soc Am. 2005; 117:934–943. [PubMed: 15759712]

52. Oelze ML, Zachary JF. Examination of cancer in mouse models using high-frequency quantitative ultrasound. Ultrasound Med Biol. 2006; 32:1639–48. [PubMed: 17112950]

53. Mamou J, Oelze ML, O'Brien WD Jr, Zachary JF. Extended three-dimensional impedance map methods for identifying ultrasonic scattering sites. J Acoust Soc Am. 2008; 123:1195–1208. [PubMed: 18247919]

54. Coron J, Mamou J, Hata M, et al. Three-dimensional segmentation of high-frequency ultrasound echo signals from dissected lymph nodes. Proceedings of the 2008 IEEE Ultrasonics Symposium. 2008:1370–1373.

55. Vlad RM, Brand S, Giles A, et al. Quantitative ultrasound characterization of responses to radiotherapy in cancer mouse models. Clin Cancer Res. 2009; 15:2067–2075. [PubMed: 19276277]

56. Vlad RM, Saha RK, Alajez NM. An increase in cellular size variance contributes to the increase in ultrasound backscatter during cell death. Ultrasound Med Biol. 2010; 36:1546–1558. [PubMed: 20800181]

57. Coron A, Mamou J, Saegusa-Beecroft E, et al. Assembling 3D histology volumes from sections of cancerous lymph nodes to match 3D high-frequency quantitative ultrasound images. Proceedings of the 2010 IEEE Ultrasonics Symposium. 2010:2368–2371.

58. Mamou J, Saegusa-Beecroft E, Coron A, et al. Three-dimensional quantitative high-frequency characterization of freshly-excised human lymph nodes. Proceedings of the 2011 IEEE Ultrasonic Symposium. 2011:27–40.

59. Lee J, Karshafian R, Papanicolau N. Quantitative ultrasound for the monitoring of novel microbubble and ultrasound radiosensitization. Ultrasound Med Biol. 2012; 38:1212–21. [PubMed: 22579547]

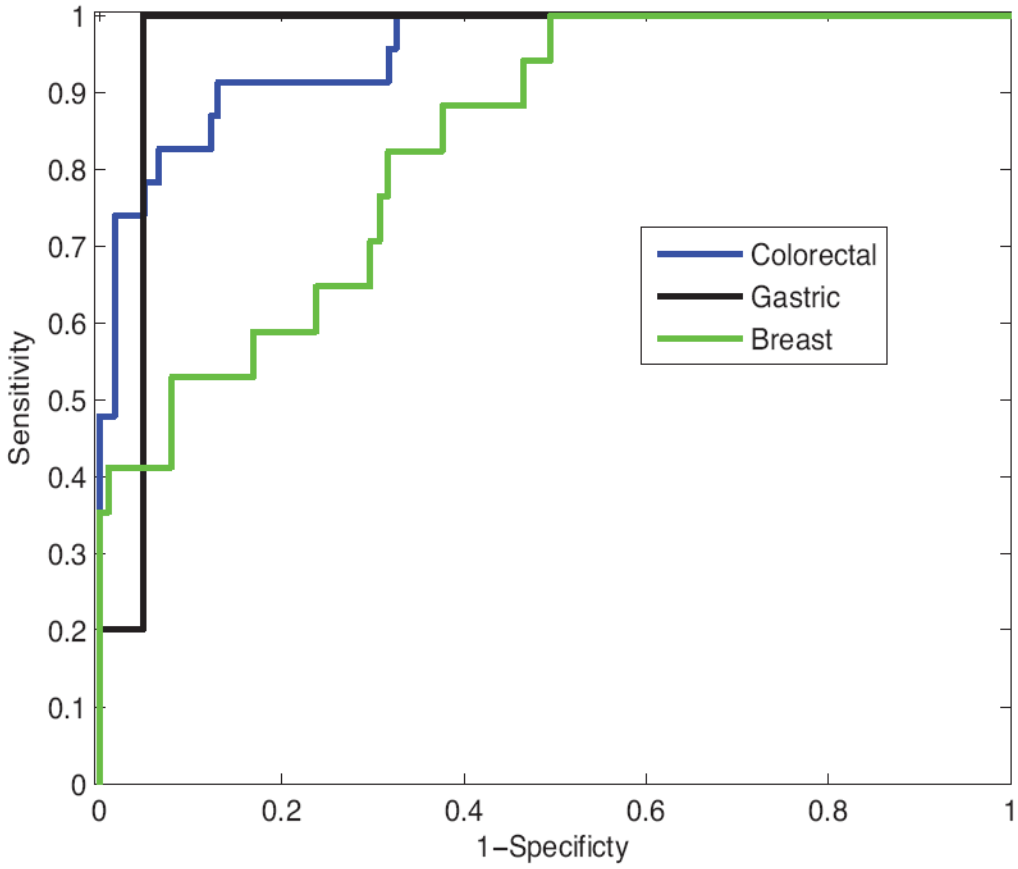

Figure 1.
Receiver-operator characteristic curves for LNs of the three cancer types. Colorectal cancer, blue line; gastric cancer, black line; breast cancer, green line. The receiver-operator characteristic curves indicate superior classification performance for colorectal and gastric cancers compared to breast cancer readily apparent.

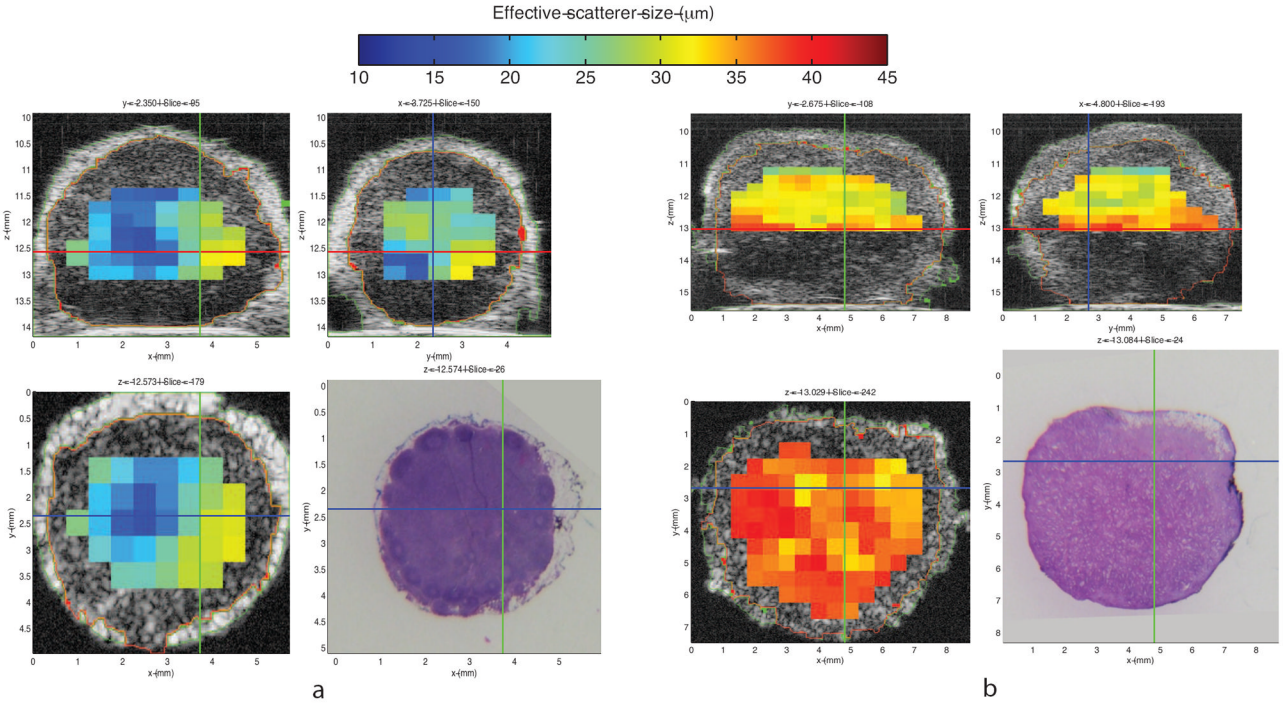

Figure 2.

Illustrative quantitative ultrasound (QUS) images: three-dimensional (3D) cross-sectional parametric images displaying effective scatterer-size estimates. Figure 2-a shows 3D cross-sectional parametric images of a benign locoregional lymph node (LN) from a colon cancer patient. Figure 2-b shows 3D cross-sectional parametric images of a locoregional LN with diffusely metastatic adenocarcinoma from a different colon cancer patient. Parametric cross-sectional B-mode images are shown with overlaid color-coded effective scatterer-size estimates. Bottom right panel of each figure displays the co-registered histology of the bottom left panel.

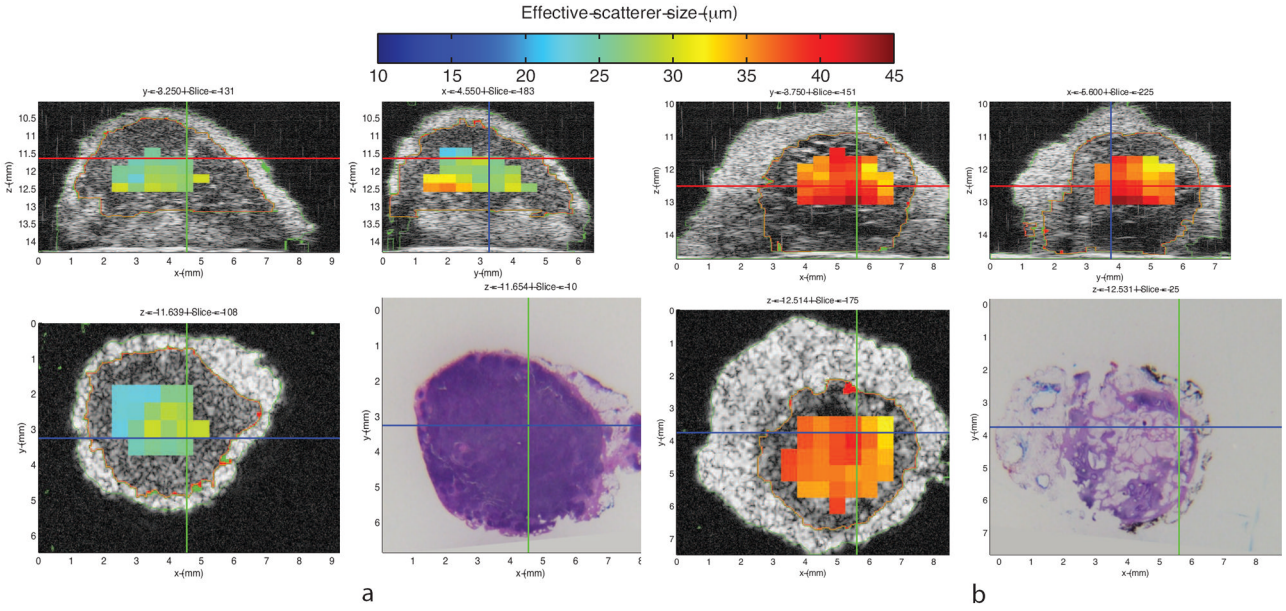

Figure 3.

Illustrative quantitative-ultrasound (QUS) images: three-dimensional (3D) cross-sectional parametric images displaying effective scatterer-size estimates. Figure 3-a shows 3D cross-sectional parametric images of a benign locoregional lymph node (LN) from a gastric cancer patient. Figure 3-b shows 3D cross-sectional parametric images of a locoregional LN with diffusely metastatic adenocarcinoma from a different gastric cancer patient. Parametric cross-sectional B-mode images are shown with overlaid color-coded effective scatterer-size estimates. Bottom right panel of each figure displays the co-registered histology of the bottom left panel.

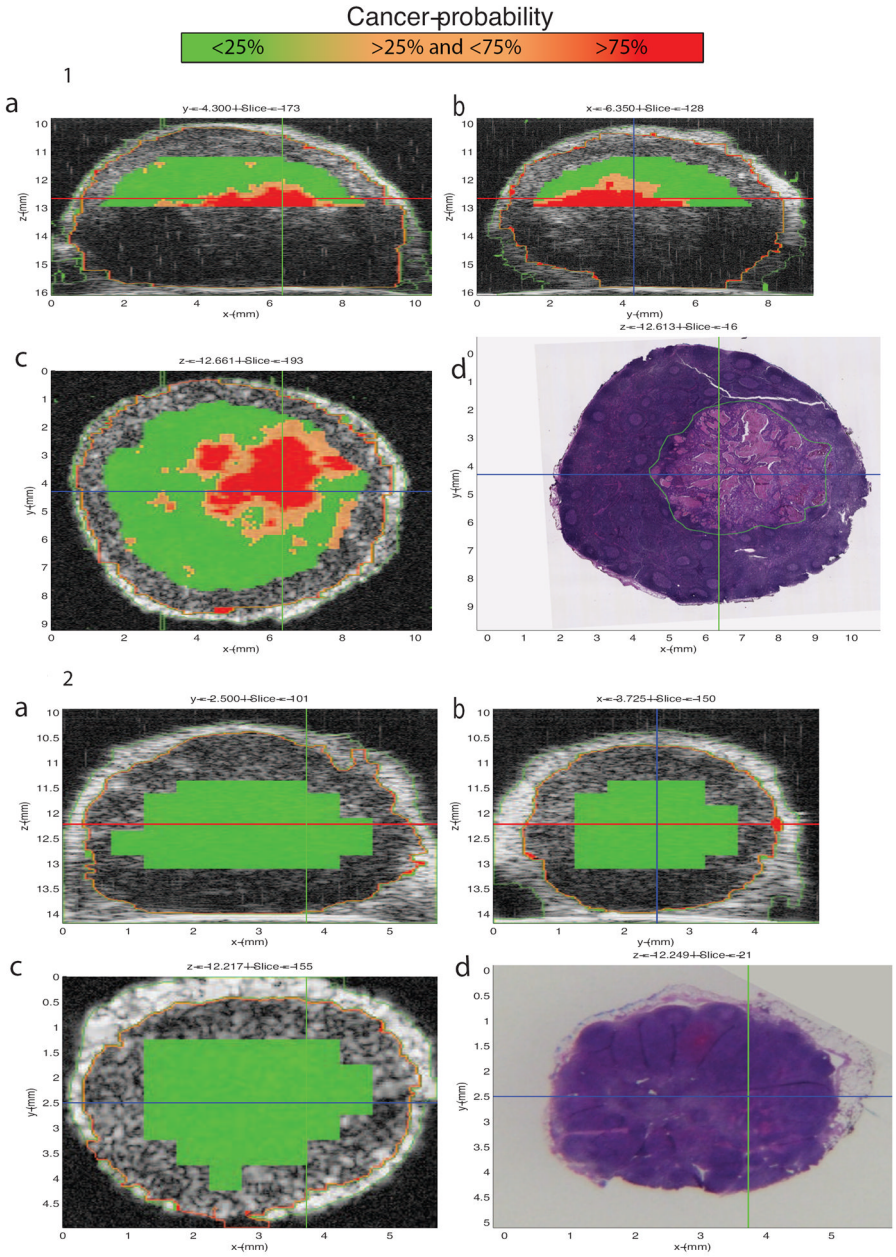

Figure 4.

1: 3D Interactive GUI with cancer-probability images of a locoregional lymph node (LN) with partially metastatic adenocarcinoma from a patient with colorectal cancer. The LN is 9.54 mm in its largest dimension, and the metastasis is 5.09 mm in its largest dimension. The graphical user interface (GUI) displays three orthogonal gray-scale B-mode cross-sections from a three-dimensional (3D) rendering in 4-1a through 4-1c. The cross sections depict color-encoded cancer-probability values using red to indicate a probability greater than 75%, orange to indicate a probability between 25 and 75%, and green to indicate a probability less than 25%. Figure 4-1d shows a co-registered hematoxylin and eosin (H&E) stained histology photomicrograph that corresponds to the same section as in 4-1c. These images show that excellent concurrence is achieved between the red cancer-probability

region and the definitive histology result shown in 4-1d showing the demarcated metastatic tumor.

2: 3D Interactive GUI with cancer-probability images of a benign locoregional lymph node (LN) with from a patient with colorectal cancer. The LN is 4.41 mm in its largest dimension. The graphical user interface (GUI) displays three orthogonal gray-scale B-mode cross-sections from a three-dimensional (3D) rendering in 4-2a through 4-2c. Figure 4-2d shows a co-registered hematoxylin and eosin (H&E) stained histology photomicrograph that corresponds to the same section shown in 4-2c. The cross sections depict color-encoded cancer-probability values using red to indicate a probability greater than 75%, orange to indicate a probability between 25 and 75%, and green to indicate a probability less than 25%. These images show that excellent concurrence is achieved between the green cancer-probability region and the definitive histology result of the benign LN shown in 4-2d.

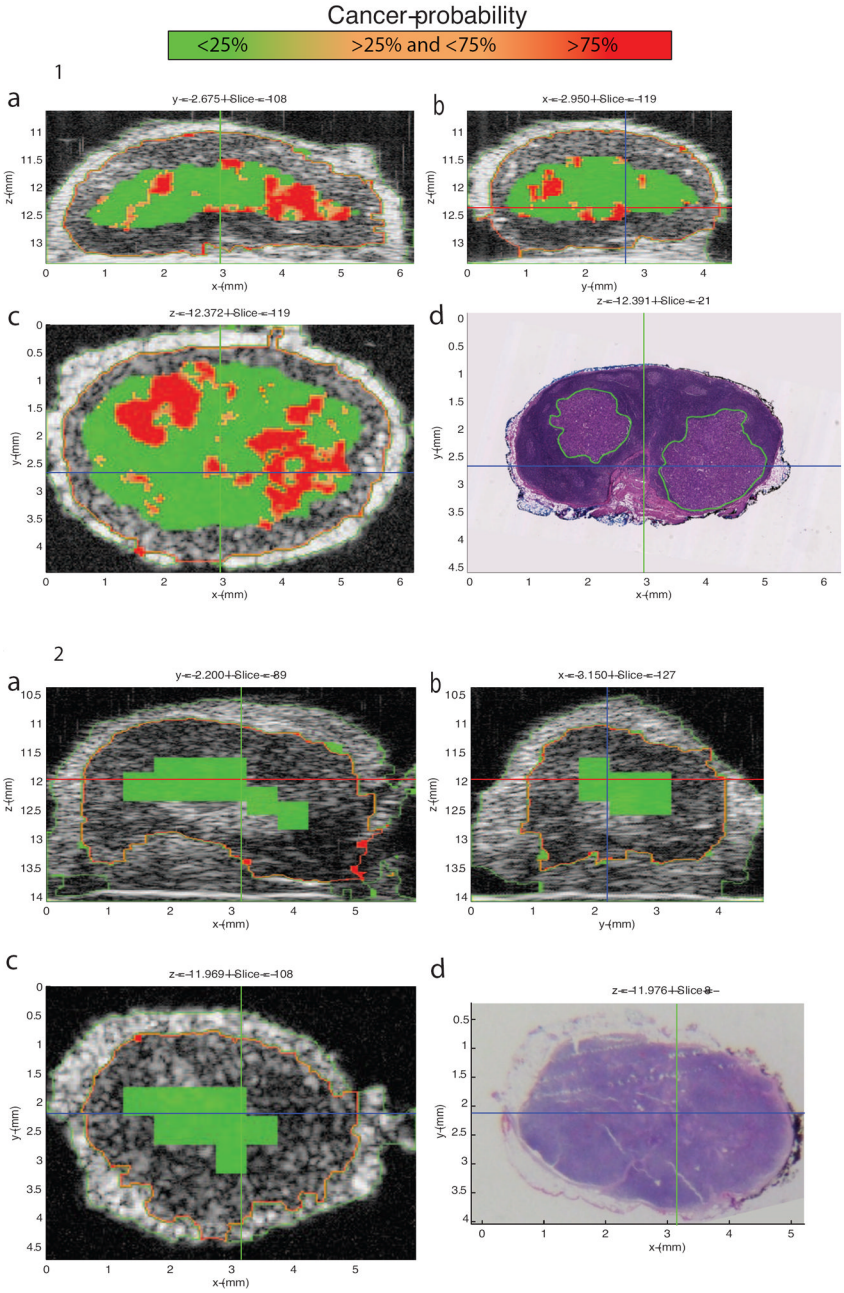

Figure 5.

1: Cancer-probability images of an axillary sentinel-lymph node (LN) of invasive ductal breast cancer patient. The LN is 5.86 mm in its largest dimension, and it contains two micrometastatic foci. The bigger focus is 1.82 mm in its largest dimension. The graphical user interface (GUI) displays three orthogonal gray-scale B-mode cross-sections from a three-dimensional (3D) rendering in 5-1a through 5-1c. The cross sections depict color-encoded cancer-probability values using red to indicate a probability greater than 75%, orange to indicate a probability between 25 and 75%, and green to indicate a probability less than 25%. Figure 5-1d shows a co-registered hematoxylin and eosin (H&E) stained histology photomicrograph that corresponds to the same section shown in 5-1c. Like Figure

4-1, Figure 5-1 shows excellent concurrence between the red high-probability region and the corresponding metastatic region in the histology result.

2: Cancer-probability images of a benign axillary sentinel-lymph node (LN) of invasive ductal breast cancer patient. The LN is 5.51 mm in its largest dimension. The cross sections depict color-encoded cancer-probability values using red to indicate a probability greater than 75%, orange to indicate a probability between 25 and 75%, and green to indicate a probability less than 25%. Like Figure 4-2, Figure 5-2 shows excellent concurrence is achieved between the green cancer-probability region and the definitive histology result of the benign LN shown in 5-2d.

Table 1

Classification performance

Cancer Type	Patients	Total LNs	Metastatic LNs	Benign LNs	Area Under the ROC Curve	95% Confidence Interval	Effective QUS Estimates	Sensitivity	Specificity
Colorectal	77	146	23	123	0.952 ±0.021	0.911 to 0.993	4 (Scatterer size, Nakagami α, Quantile-quantile Sa, Quantile-quantile Cy)	100.00%	67.50%
								91.30%	87.00%
Gastric	12	26	5	21	0.962 ±0.039	0.807 to 1.000	3 (Scatterer size, Intercept, Homodyned-K *k*)	100.00%	95.30%
Breast	71	118	17	101	0.833 ±0.047	0.741 to 0.926	4 (Scatterer size, Slope, Quantile-quantile Cy, Homodyned-K μ)	100.00%	50.50%
								88.20%	62.50%